Received: 10 October 2022 | Revised: 3 July 2023 | Accepted: 21 August 2023

DOI: 10.1002/joc.8241

International Journal of Climatology RMetS

RESEARCH ARTICLE

The efficacy of tropical and extratropical predictors for long-lead El Niño-Southern Oscillation prediction: A study using a machine learning algorithm

Wan-Jiao Song[1,2,3] | **Jin-Yi Yu**[4] | **Tao Lian**[2]

[1]Key Laboratory of Radiometric Calibration and Validation for Environmental Satellites, National Satellite Meteorological Center (National Center for Space Weather), China Meteorological Administration, Beijing, China

[2]State Key Laboratory of Satellite Ocean Environment Dynamics, Second Institute of Oceanography, Hangzhou, China

[3]Innovation Center for FengYun Meteorological Satellite (FYSIC), Beijing, China

[4]Department of Earth System Science, University of California, Irvine, California, USA

Correspondence
Wan-Jiao Song, Key Laboratory of Radiometric Calibration and Validation for Environmental Satellites, National Satellite Meteorological Center (National Center for Space Weather), China Meteorological Administration, Beijing 100081, China.
Email: songwj90@163.com

Funding information
National Natural Science Foundation of China, Grant/Award Number: 41801355; NSF's Climate and Large-Scale Dynamics Program of USA, Grant/Award Number: AGS-2109539; Open Fund of State Key Laboratory of Satellite Ocean Environment Dynamics, Second Institute of Oceanography, Grant/Award Number: QNHX2213

Abstract

This study illustrates the considerable improvement in accuracy achievable for long-lead forecasts (18 months) of the Ocean Niño Index (ONI) through the utilization of a long short-term memory (LSTM) machine learning algorithm. The research assesses the predictive potential of eight predictors from both tropical and extratropical regions constructed based on sea surface temperature, outgoing longwave radiation, sea surface height and zonal and meridional wind anomalies. In comparison to linear regression model forecasts, the LSTM model outperforms them for both the tropical and extratropical predictor sets. Among all the predictors, the western North Pacific (WNP) index demonstrates the highest prediction skill in ONI forecasts, followed by the North Tropical Atlantic (NTA) index and then the sea surface height index. While other predictors help the LSTM model to forecast either the phase variation of the amplitude variation of the observed ONI, the extratropical WNP predictor enables the LSTM model to forecast both variations. This superiority can be attributed to the involvement of SST anomalies in the WNP region in both tropical and extratropical El Niño–Southern Oscillation (ENSO) dynamics, allowing for the utilization of predictive potential from both components of ENSO dynamics. The study also concludes that the extratropical ENSO dynamics provide a robust source of predictability for long-lead ENSO forecasts, which can be effectively harnessed using the LSTM model.

KEYWORDS
ENSO, extratropical predictors, machine learning and tropical

1 | INTRODUCTION

The El Niño–Southern Oscillation (ENSO) is a large-scale combined phenomenon of fluctuating marine and atmospheric circulation over the Pacific Ocean. These fundamental processes governing the evolution of ENSO events are primarily concentrated at tropical Pacific (Neelin, 1991; Philander, 1998; Wang, 2018). These

processes involve complex interactions among atmospheric properties, surface ocean properties and subsurface ocean properties. Many ENSO statistical schemes and physical prediction models have predominantly utilized tropical atmospheric and oceanic properties in predicting typical ENSO indices on lead times of 6 months (Barnston et al., 2019; Jin & Kinter, 2009; Latif et al., 1998). These models have demonstrated skilful seasonal dependence in predictability of ENSO process. In recent decades, the performance of ENSO prediction models has declined (Barnston et al., 2012). This may be attributed to changes in the properties and dynamics of ENSO (Capotondi et al., 2015; Yu et al., 2012, 2017), which have rendered traditional tropical predictors less effective in forecasting ENSO events. To restore the previous level of skill, it may be necessary to incorporate additional predictors into ENSO prediction models.

During the past two to three decades, ENSO events have exhibited a notable shift in their spatial characteristics. Instead of having the largest sea surface temperature (SST) anomalies in the tropical eastern Pacific as observed in the majority of ENSO events in the 20th century, recent ENSO events have shown their most prominent SST anomalies in the tropical central Pacific. This distinction has sparked significant interest in studying the central Pacific (CP) and eastern Pacific (EP) ENSOs (Kao & Yu, 2009; Yu & Kao, 2007). Several studies have highlighted the potentially greater influence of the extratropical Pacific, particularly in the case of CP ENSO events (Yu et al., 2010, 2017; Yu & Kim, 2011). ENSO precursors have been identified not only in the tropical Pacific but also in the extratropical Pacific. SST anomalies in the eastern and western North Pacific, for instance, have been recognized as precursors to ENSO events (Pegion et al., 2020; Wang et al., 2012; Yu et al., 2010; Yu & Kim, 2011). Similarly, variables in the extratropical regions of other ocean basins can serve as ENSO precursors. For example, temperature anomalies in the North Tropical Atlantic during boreal spring have been shown to trigger ENSO events (Ham et al., 2013a, 2013b; Wang et al., 2017). These recent studies suggest that both tropical and extratropical ocean-atmospheric predictors from the Pacific and other ocean basins hold potential for ENSO prediction and can be integrated into ENSO forecast models to enhance prediction skill.

ENSO predictions are typically carried out using statistical schemes and dynamical models. Statistical schemes are simpler and computationally less demanding compared to dynamical models. Conventional statistical models struggle to capture the nonlinear aspects of ENSO dynamics (Pegion et al., 2020; Timmermann et al., 2018). In recent years, there have been several attempts to utilize machine learning for ENSO forecasts. Machine learning algorithms have shown greater potential than conventional statistical methods in capturing the nonlinear characteristics and addressing challenges such as the spring predictability barrier (Chen et al., 2021; Nooteboom et al., 2018). One particular machine learning technique is the long short-term memory (LSTM) neural network model, which can be constructed by integrating ensemble empirical mode decomposition with a convolutional neural network on occasion. LSTM models have demonstrated skill in producing accurate El Niño index forecasts (Guo et al., 2020; Gupta et al., 2022; He et al., 2017). However, none of these previous studies examined the predictability or prediction of ENSO using full collection of multiple marine and atmospheric, tropical and extratropical, the Pacific and Atlantic Ocean precursors. In the present study, to categorize more objectively the candidate and core variables associated with the extreme phases of the ENSO forcing, a set of LSTM machine learning technique and linear regression statistical methods were employed for determining the efficacy of ENSO-related marine and atmospheric signal precursors. The main objective of this study is to examine whether there are any systematic differences in the predictive capabilities of tropical and extratropical predictors in ENSO forecasts and to understand the underlying reasons.

2 | DATA AND METHODS

Various marine and atmospheric products are used in this study, which are listed in Table 1 for reference. Specifically, the SST data is obtained from the NOAA Extended Reconstructed Sea Surface Temperature V4 dataset (Huang & Xie, 2015). The interpolated outgoing long-wave radiation (OLR) data (Liebmann & Smith, 1996) is utilized, along with zonal wind and meridional wind (U-wind and V-wind, respectively) data from the National Centers for Environmental Prediction-National Centre for Atmospheric Research Reanalysis (Kalnay et al., 1996). Sea surface height (SSH) data is sourced from the National Centers for Environmental Prediction Global Ocean Data Assimilation System (Behringer & Xue, 2004). All datasets have been re-gridded to a uniform 2.5° × 2.5° horizontal resolution and are available monthly. The Ocean Niño Index (ONI) is derived from the National Centers for Environmental Prediction, part of the National Oceanic and Atmospheric Administration. Anomalies in this study are calculated by subtracting the long-term monthly average over the analysis period. Linear trends were removed using the linear least squares fit in time. The traditional Niño3.4 index, based on monthly SST anomalies over the Niño3.4 region (5°S–5°N, 170°–120°W), is also computed. The study period spans from 1982 to 2021 to ensure that all necessary atmospheric and marine variables are available.

TABLE 1 Monthly reanalysis products utilized in this study

Var.	Data source	Span	Spatial res.	Unit
SST	ERSST V4 (Huang et al., 2016)	Jan 1854–Feb 2022	1° × 1°	°C
SSH	GODAS (Behringer & Xue, 2004)	Jan 1980–Dec 2019	1/3° × 1°	m
OLR	NOAA/PSD (Liebmann & Smith, 1996)	Jun 1974–Dec 2019	2.5° × 2.5°	$W \cdot m^{-2}$
U-wind	NOAA/PSD (Kalnay et al., 1996)	Jan 1948–Dec 2020	2.5° × 2.5°	$m \cdot s^{-1}$
V-wind	NOAA/PSD (Kalnay et al., 1996)	Jan 1948–Dec 2020	2.5° × 2.5°	$m \cdot s^{-1}$
ONI	NOAA/CPC	Jan 1950–Feb 2022		°C

Abbreviations: ONI, Ocean Niño Index; OLR, outgoing longwave radiation; SSH, sea surface height; SST, sea surface temperature; *U*-wind, sea surface zonal wind; *V*-wind, sea surface meridional wind.

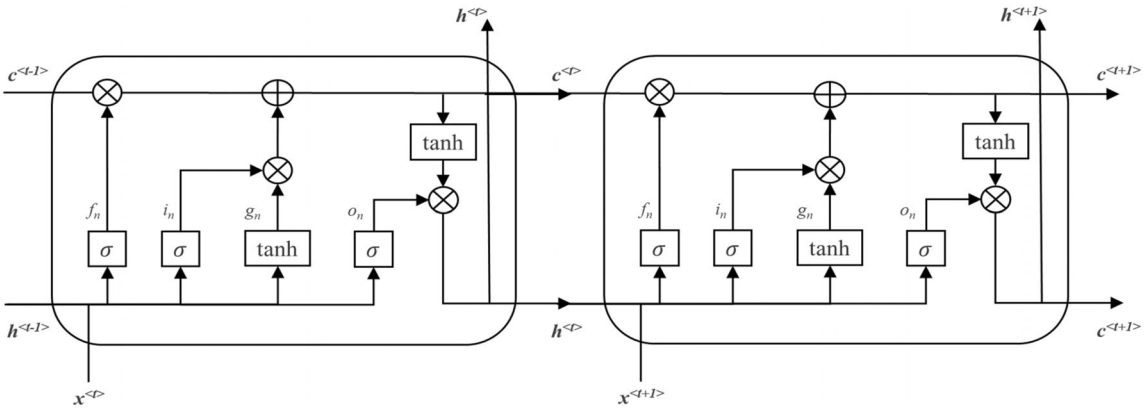

FIGURE 1 Structure diagram of the long short-term memory neural network. Here, ⊗ represents multiple, ⊕ represents plus. σ represents sigmoid function, which ranges [0, 1]. tan*h* represents tan*h* function, which is used as the active function in the normal neural network. $x^{<t>}$ represents the input data. $h^{<t-1>}$ represents the history data information computed by the last neuron. $h^{<t>}$ represents the data computed by this neuron. $c^{<t-1>}$ represents the memory data from last neuron. $c^{<t>}$ represents the memory data after processing by this neuron

Complex neural networks and machine learning techniques are highly effective in analysing large volumes of data. Of the recurrent neural networks available, long short-term memory networks are particularly noteworthy. One main advantage of recurrent neural networks is their interconnected inputs, which can capture the interactions among multiple variables involved in the ENSO phenomenon. LSTM networks are designed to retain short-term valuable information in memory for long-term utilization, making them suitable for ENSO forecasting (Behringer & Xue, 2004; Guo et al., 2020; Huang et al., 2019; Huang & Xie, 2015; Kalnay et al., 1996; Liebmann & Smith, 1996). Figure 1 illustrates the components of the LSTM network, which comprise a memory cell and three distinct gates: the input gate, forget gate and output gate. These gates are crucial for updating, maintaining and deleting information within the cell state. The calculation process of the LSTM network can be expressed through Equations (1)–(5),

$$\text{Forget gate} \quad f^{<t>} = \sigma\left(W_{xf}x^{<t>} + W_{hf}x^{<t-1>} + b_f\right), \tag{1}$$

$$\text{Input gate} \quad i^{<t>} = \sigma\left(W_{xi}x^{<t>} + W_{hi}x^{<t-1>} + b_i\right), \tag{2}$$

$$\text{Output gate} \quad o^{<t>} = \sigma\left(W_{xo}x^{<t>} + W_{ho}h^{<t-1>} + b_o\right), \tag{3}$$

$$\text{Neutron} \quad c^{<t>} = f^{<t>} \odot c^{<t-1>} + i^{<t>} \odot \tan h \left(W_{xc}x^{<t>} + W_{hc}h^{<t-1>} + b_c\right), \tag{4}$$

$$\text{Objective function} \quad h^{<t>} = o^{<t>} \tan h \odot (c^{<t>}), \tag{5}$$

$$\text{MSE} = \frac{1}{n}\sum_{1}^{n}\left(Y_i - \widehat{Y}_i\right)^2. \tag{6}$$

In the context of this study, the symbol ⊗ represents multiple and ⊕ represents plus. σ represents the sigmoid function, which yields values in the range of [0, 1].

The symbol tan$h$ corresponds to the hyperbolic tangent function, employed as the activation function in conventional neural network. $c^{<t-1>}$ denotes the memory data received from previous neuron, whereas $x^{<t>}$ represents the input data. $h^{<t-1>}$ signifies the historical information computed by the preceding neuron and $h^{<t>}$ denotes the data computed by the current neuron. The processed memory data by this neuron is denoted as $c^{<t>}$. n signifies the number of samples. Y_i represents the actual value, whereas $\widehat{Y}_i$ denotes the predicted value.

Previous studies have indicated that training models can be prone to overfitting when the available training data is limited (Guo et al., 2020; McPhaden et al., 2015; Srivastava et al., 2014). In order to address this issue, dropout rates are utilized as a means of mitigating overfitting. To determine the optimal dropout rate, a range of dropout rates was selected for comparison. The training experiments were conducted using dropout rates of 0.1, 0.2, 0.3, 0.4 and 0.5, with a dropout rate of 0.5 demonstrating superior training performance. Furthermore, different combinations of cell numbers (24, 36, 48) and iterator numbers (100, 120, 150, 180, 200) were tested to evaluate their impact on training. The results indicated that the best training performance was achieved when the cell number was set to 24 and the iterator number was set to 100. For climate indices forecasting, a monthly time step with a step size of 18 was employed. The mean square error (MSE) served as the loss function to evaluate the performance of the LSTM model (Equation (6)). To ensure consistency and comparability, both the training set (1982–2013) and the validation set (2014–2021) underwent standardization using the Z-score method. The analysis was performed on a test data set covering the period from 1982 to 2021. Additionally, we examined the correlation coefficient (R), root-mean-square error (RMSE) and standard deviation (SD) to evaluate the performance of different linear regression statistical schemes and machine learning models in terms of discrimination and calibration. The optimal predictive model was selected based on minimal root mean squared error and maximal correlation coefficient over the leave eight out cross-validated datasets.

3 | EXPERIMENT DESIGN AND RESULTS

3.1 | Identification of precursors

Selecting the appropriate attributes based on the evolution of ENSO is crucial for improving the efficiency of ENSO prediction using machine learning techniques. It provides a physical basis for essential information to make accurate predictions. Network variables offer global information on building correlations to help predict ENSO events. This study employed a total of eight air–sea variable-based indices as precursors for ENSO prediction. The ONI serves as the target forecasting index. The definitions of the eight precursors are indicated in Table 2, which include five tropical precursors and three

TABLE 2 Definitions of the Niño indices and their precursors from both the tropical and extratropical Pacific oceans: (1) tropical SST index, defining sea surface temperature anomalies in the Niño3–Niño4 region; (2) tropical SSH index, outlining sea surface height anomalies in the tropical Niño3–Niño4 region; (3) tropical OLR index, investigating outgoing longwave radiation anomalies over the tropical central Pacific; (4) tropical U-wind index, examining zonal wind anomalies in the tropical Niño3–Niño4 region; (5) tropical V-wind index, detailing meridional wind anomalies in the tropical Niño3–Niño4 region; (6) NTA index, characterizing sea surface temperature anomalies over the north tropical Atlantic; (7) extratropical WNP index, exploring sea surface temperature anomalies over the western North Pacific; and (8) extratropical SPQ index, investigating sea surface temperature anomalies over the South Pacific

Predictors	Definitions	References
SST index	SST anomaly in Niño4 and Niño3 areas (160°E–90°W, 5°S–5°N)	Trenberth and Stepaniak (2001)
SSH index	SSH anomaly (160°E–90°W, 5°S–5°N)	Trenberth and Stepaniak (2001)
OLR index	OLR anomaly (160°E–160°W, 5°S–5°N)	Ma et al. (2010)
U-wind index	Zonal wind anomaly (160°E–90°W, 5°S–5°N)	Trenberth and Stepaniak (2001)
V-wind index	Meridional wind anomaly (160°E–90°W, 5°S–5°N)	Trenberth and Stepaniak (2001)
North tropical Atlantic (NTA) index	SST anomaly (EQ–15°N, 90°W–20°E)	Ham et al. (2013a, 2013b)
Western North Pacific (WNP) index	SST anomaly (90°E–150°W, 10°S–30°N)	Modified from Wang et al. (2012) and Pegion et al. (2020)
South Pacific quadrupole (SPQ) index	SST anomaly (150°E–75°W, 20°S–65°S)	Ding et al. (2015), Qin et al. (2017) and Pegion et al. (2020)

extratropical ENSO precursors. Figure 2 displays the major domains of the tropical and extratropical ENSO precursors, superimposed on the SST anomalies regressed onto the ONI during the boreal winter (December–January–February). The specific longitude–latitude regions utilized to define these indices are outlined in Table 2.

The tropical precursors include indices that represent SST, SSH, *U*-wind and *V*-wind anomalies averaged in different regions of the tropical Pacific (see the region information provided in Table 2). These indices were used to represent ocean–atmosphere interactions over the tropical Pacific. Additionally, a tropical OLR index is included to account for the potential influence of tropical deep convection, as represented by variations in OLR (Ma et al., 2010). Different extratropical precursors have been identified in the literature using various definitions. Basin-wide interactions between the tropical and extratropical Pacific have also been shown to affect ENSO events by processes in the extratropical northern and southern Pacific in previous studies (Pegion et al., 2020; Yu et al., 2010; Zhang et al., 2014). As previously mentioned, SST anomalies in the northern tropical Atlantic region can also affect the evolution of ENSO through interbasin interactions with the extratropical Pacific (Ham et al., 2013a; Ren et al., 2019; Wang et al., 2017). These extratropical processes are referred as the subtropical ENSO dynamics (Yu & Fang, 2018) and are referred to as the extratropical ENSO dynamics here. We choose to use three extratropical precursors to represent the extratropical ENSO dynamics. They respectively represent SST anomalies over the North Tropical Atlantic (NTA), western North Pacific (WNP) and South Pacific (SPQ).

A correlation heat map is used to evaluate the simultaneous relationships between the ONI and the eight selected precursors (Figure 3). The ONI exhibits stronger correlations with almost all the tropical indices (SST, OLR, SSH and *U*-wind), except for the *V*-wind index. These variables are intercorrelated but not independent. In contrast, the ONI exhibits weak correlations with the extratropical indices (WNP and SPQ), with the exception of the NTA index. The simultaneous correlations between the ONI and the extratropical WNP and SPQ indices are close to zero. Although the WNP and *V*-wind indices show weak direct correlations with the ONI, they display measurable correlations with the group of indices that have high direct correlations with the ONI. The WNP index exhibits measurable correlations with the SSH and NTA indices, while the *V*-wind index displays measurable correlations with the SSH, OLR and *U*-wind indices. The northern Pacific (i.e., the WNP index), southern Pacific (i.e., the SPQ index) and tropical Atlantic Ocean (i.e., the NTA index) are not highly correlated with each other, indicating that the distinct basin could provide independent information in predicting

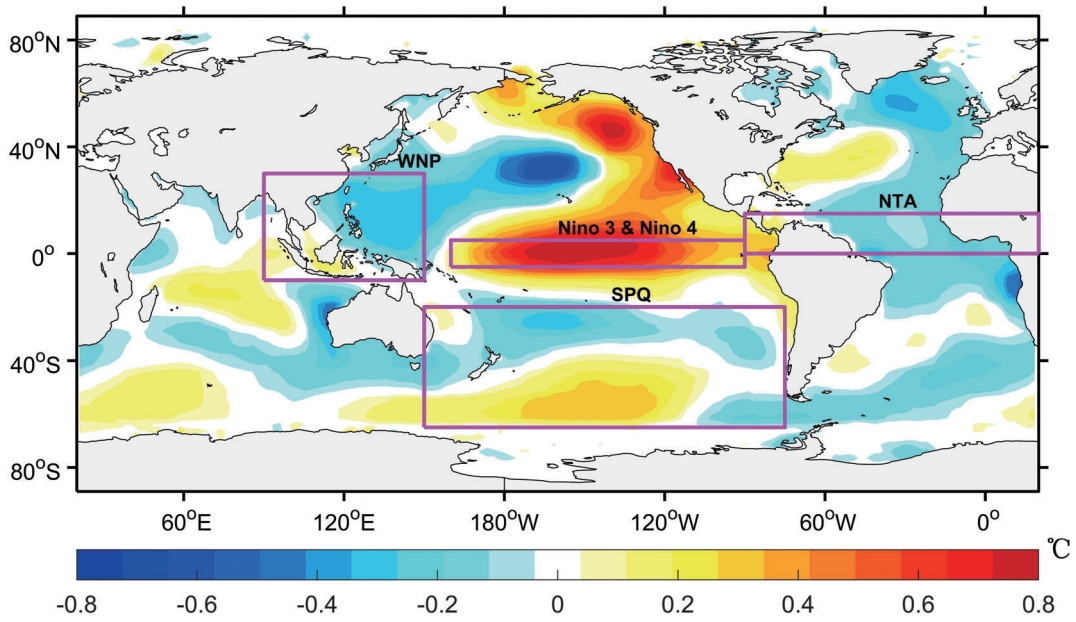

FIGURE 2 Domains of tropical and extratropical ENSO precursors are depicted in the figure. The colour shading represents sea surface temperature anomalies in DJF (December–January–February) regressed onto the Ocean Niño Index from 1983 to 2019. Detailed information regarding the data sets and the exact longitudes–latitudes of the domains for calculating the precursors can be found in Tables 1 and 2. The WNP stands to the western North Pacific, NTA stands for the North tropical Atlantic, and SPQ stands for the South Pacific quadrupole [Colour figure can be viewed at wileyonlinelibrary.com]

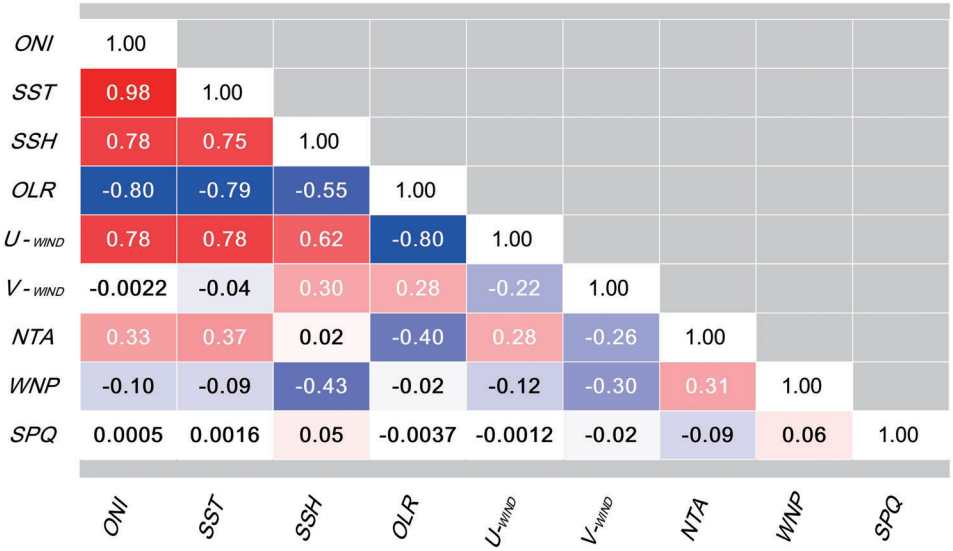

FIGURE 3 A heatmap is presented, illustrating the simultaneous correlation coefficients between the Ocean Niño Index (ONI) and the eight predictors over the period of 1982–2019. The predictors include the tropical Pacific sea surface temperature (SST), sea surface height (SSH), outgoing longwave radiation (OLR), sea surface zonal wind (*U*-wind), and meridional wind (*V*-wind), as well as SST indices for the North Tropical Atlantic (NTA), western North Pacific (WNP), and South Pacific (SPQ) (see Table 2 for details). Positive correlations are represented by red shadings, while negative correlations are denoted by blue shadings. The intensity of the colour shading indicates the magnitude of the correlation, with darker shades indicating higher magnitudes [Colour figure can be viewed at wileyonlinelibrary.com]

ENSO phenomenon. Through intercorrelations among the predictors, all eight predictors have the potential to affect ENSO predictions.

3.2 | Performance of the LSTM model

To determine the overall performance, eight predictor combinations were assessed. The LSTM algorithm's effectiveness for predicting ONI was analysed using two methods: employing the tropical Pacific SST index as the sole predictor, and combining the SST index with one of the other seven Table 2 indices. The "SST-only LSTM" represented the utilization of LSTM exclusively to monthly SST anomalies in the Niño3 and Niño4 areas. The performance of the LSTM and regression models was evaluated in Figure 4, considering the correlation coefficient (R), root-mean-square error (RMSE) and standard deviation (SD) between the forecasted and observed ONI values throughout the entire forecasting period from 1983 to 2021. In this discussion, our focus is on comparing the correlation coefficient values. At the 18-month lead time, there was a significant divergence in performance between the LSTM and regression models, as depicted in Figure 4. The LSTM model outperformed the regression model in all eight predictor combinations, including the scenario where the tropical SST index was the only predictor. The correlation coefficient between the forecasted and observed ONI values for the LSTM model was 0.73, whereas the regression model yielded a correlation of 0.22. This improvement indicates the LSTM model's superior ability, relative to linear regression, to leverage the prediction potential of the tropical SST index for forecasting the ONI. The LSTM algorithm successfully addresses the problem of vanishing gradients by retaining the available information and ignoring the unavailable information (Guo et al., 2020). Linear regression models, in contrast, are restricted in capturing only linear relationships between predictors and ENSO indices (Pegion et al., 2020).

Including the tropical SSH index as the second predictor in the LSTM model results in a skill increase to $R = 0.76$ (Figure 4). This improvement aligns with the delayed or recharged oscillator theories of ENSO (Battisti & Hirst, 1989; Cane & Zebiak, 1985; Jin, 1997; Suarez & Schopf, 1988), which depict the tropical ENSO dynamics and illustrate that ENSO-related subsurface thermocline variation in the tropical Pacific (represented by the SSH index) displays a lead-lagged correlation with tropical SST variation, instead of a simultaneous one. Yu and Fang (2018) have previously emphasized the semi-periodic ENSO evolution that characterizes the tropical ENSO dynamics through the interaction between tropical SST, wind and SSH variations. The semiperiodic nature of the ENSO cycle may be better identified by machine learning algorithms, enabling more accurate

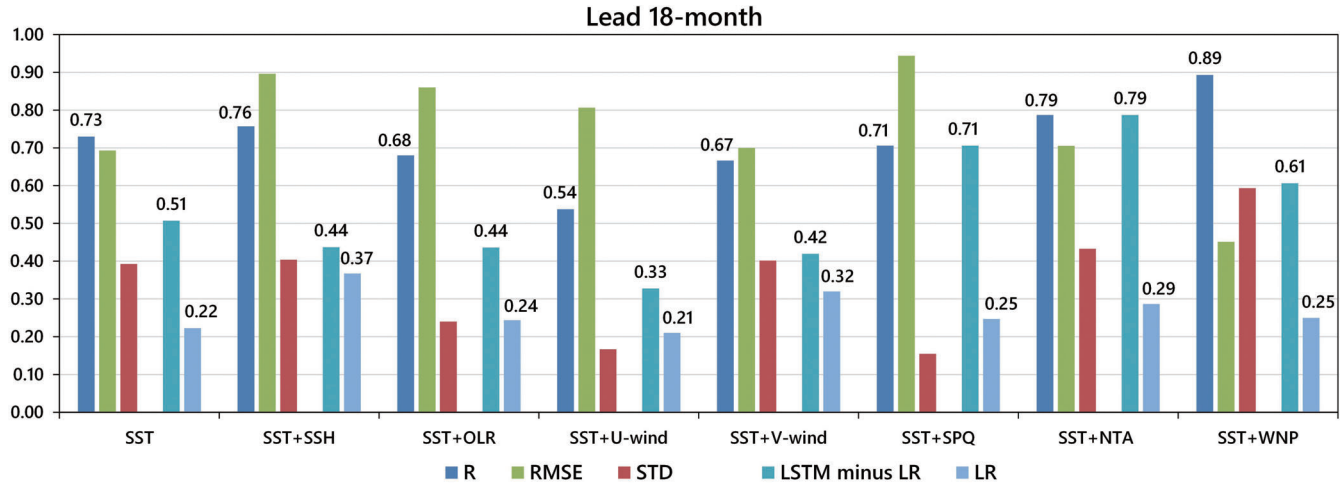

FIGURE 4 Performances of the long short-term memory network (LSTM) and linear regression (LR) models at their 18-month lead time forecasts. The performances are evaluated based on assessing the correlation coefficient (R), root-mean-square error (RMSE) and standard deviation (SD) between the forecasted and observed ONI values during the entire forecasting period (1983–2021) for eight groups of precursor combinations. The LR bars indicate the performance of the LR model based on the correlation value, while the LSTM minus LR bars indicate the difference in correlation coefficients between the LSTM and LR models. Table 2 provides detailed information about all eight predictors analysed in this study [Colour figure can be viewed at wileyonlinelibrary.com]

predictions at longer lead times than at shorter lead times. The periodic nature of ENSO is attributed to the cyclic oscillation between the El Niño and La Niña phases. These phases are characterized by lagged thermocline responses of SSH to surface wind forcing, which are distinguishing features of ENSO. Therefore, incorporating both the tropical SSH index and the tropical SST index offers superior forecast performance relative to incorporating other tropical indices (such as OLR, U and V) for multivariable forecasting.

As shown in Figure 4, the LSTM model performs best with extratropical predictors combined with the tropical SST index at 18-month lead times. Specifically, the LSTM model exhibits significantly better performance during the 18-month forecast, with R-value ranging between 0.71 and 0.89 when implementing the SPQ, NTA and WNP indices with the tropical SST predictor, compared to tropical predictors, which generate an R-value range of 0.54–0.76 when U-wind, OLR and SSH indices are employed. Interestingly, the WNP index, which represents a dipole SST over the western North Pacific, serves as a notable predictor of El Niño occurrences in the Northern Hemisphere. The investigation discovered that WNP produced the most effective predictive results ($R = 0.89$) for forecasting the ONI, followed by the NTA index ($R = 0.79$), and subsequently by the SPQ index ($R = 0.71$). These findings highlight the value of utilizing extratropical processes linked with the three indices to forecast the ONI at extended lead times. These results are aligned with prior research that posited that extratropical Pacific atmospheric variability influences ENSO evolution through a seasonal footprint mechanism during the pre-ENSO winter, thereby impacting spring and summer conditions in subsequent years (Di Lorenzo et al., 2010; Vimont et al., 2003; Yu et al., 2010). Precursors to ENSO in the extratropical North Pacific offer additional and diverse sources of ENSO predictability (Bruce et al., 2013; Zhao et al., 2021). It is noteworthy to observe the significant efficacy of the NTA index in facilitating an extended lead time for ENSO predictions using machine learning algorithms. As previously indicated, NTA SST anomalies play a role in commencing ENSO events by means of interbasin interactions, thus providing an extra prediction potential beyond the tropical SST index. These findings demonstrate the capability of machine learning algorithms to identify and exploit nonlinear correlations inherent in interbasin interactions between ENSO and adjacent oceans for ENSO prediction.

3.3 | Ocean Niño Index evolutions forecasted using tropical and extratropical predictors

Figure 5 compares the time series of monthly observed ONI values and 18-month forecasts using various predictor combinations, including the tropical SST index alone, as well as four multivariable combinations (SST + SSH, SST + SPQ, SST + NTA and SST + WNP). In Figure 5a,

the LSTM model forecasts the temporal evolution of the ONI using only the tropical SST index as the predictor. While the LSTM model reasonably predicts the phase variation of the observed ONI, the forecasted ONI intensity appears to be too weak. The standard deviation of the forecasted ONI is 0.12°C, representing only 13% of the observed ONI's standard deviation (0.88°C). The high correlation coefficient of 0.73 shown in Figure 4 for the SST-only forecast mainly arises from the accurate prediction of the ONI's phase variation rather than its amplitude variation. When the tropical SSH index is included in the prediction (SST + SSH), the LSTM model more accurately forecasts the amplitude variation of the observed ONI. The standard deviation of the forecasted ONI for the combined SST + SSH is 0.40°C, which accounts for 45% of the observed ONI's standard deviation. However, the forecasted phase variation is weaker compared to the observed phase variation. Thus, the high correlation coefficient of 0.76 shown in Figure 4 for the combined SST + SSH forecast primarily stems from the accurate prediction of the ONI's amplitude variation rather than its phase variation.

Notably, combining the tropical Pacific SST index with the extratropical WNP predictor (Figure 5b) significantly improves the LSTM model's forecasting capabilities for both the amplitude variation and phase variation of the ONI. The standard deviation of the forecasted ONI reaches 0.59°C, equivalent to 67% of the observed ONI's standard deviation. The phase variation of the forecasted ONI also closely matches the observed phase variation. This synergy is the key reason why the LSTM model performs exceptionally well when using the SST + WNP combination for the 18-month lead forecast, achieving a correlation coefficient as high as 0.89 between the forecasted and observed ONI values (see Figure 4). In contrast, the other two extratropical precursors (NTA and SPQ)

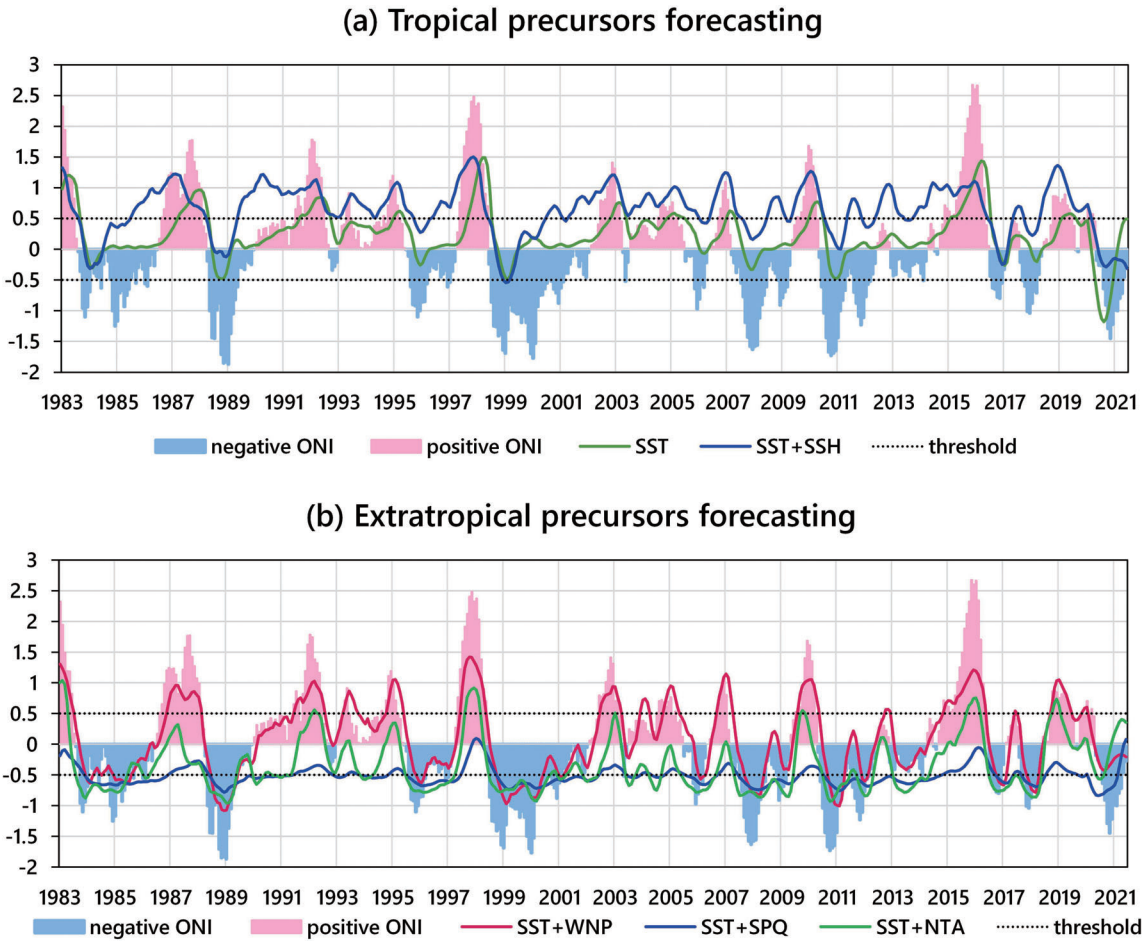

FIGURE 5 Monthly time series of the observed Ocean Niño Index (ONI) values (pink and blue shading) and the corresponding 18-month predicted values (line). These forecasts were generated using the long short-term memory neural network (LSTM) model by employing various predictor combinations, including: (a) tropical sea surface temperature (SST) index, tropical SST and sea surface height (SSH) indices. (b) tropical SST and SST over the western North Pacific (WNP) indices, tropical SST and SST over the South Pacific (SPQ) indices, tropical SST and SST over the North Tropical Atlantic (NTA) indices [Colour figure can be viewed at wileyonlinelibrary.com]

enable the LSTM model to forecast the overall phase variation of the observed ONI but not the observed amplitude variation. The standard deviation of the forecasted ONI is 0.43°C when using the SST + NTA combination, whereas it reduces to only 0.15°C when using the SST + SPQ combination (see Figure 5b). This explains why the performance of the LSTM model in the 18-month forecast is better with the SST + NTA combination (correlation coefficient $R = 0.79$) compared to the SST + SPQ combination (correlation coefficient $R = 0.71$).

Based on our analysis results, it is evident that the extratropical WNP predictor surpasses all other predictors in enabling the LSTM model to realistically forecast the amplitude variation of ENSO events. These findings suggest that the ability to forecast the amplitude variation of the ONI, rather than the phase variation, is crucial in determining the efficacy of a predictor in long-lead forecasts, such as the 18-month lead time.

4 | PHYSICAL MECHANISMS LINKING THE TROPICAL AND EXTRATROPICAL PREDICTORS TO OCEAN NIÑO INDEX EVOLUTION

Figure 6 presents the lead-lagged correlations between the ONI index and the SST or SSH anomalies within the regions where three key predictors (SSH, WNP and NTA indices) were defined, aiming the provide insights into the physical mechanisms linking these tropical and extratropical predictors to the evolution of the ONI. In this context, the SSH index serves as a tropical precursor, the NTA as an extratropical precursor and the WNP as the predictor that yields the highest performance in 18-month lead forecasts for the LSTM model.

Figure 6a showcases the correlations between the ONI and SSH anomalies along the equatorial (5°S–5°N) eastern-to-central Pacific. The correlations reveal that approximately 18 months prior to the ONI peak (at lag 0), positive SSH anomalies emerge in the tropical western Pacific and subsequently propagate eastward, triggering El Niño in the tropical central-to-eastern Pacific. This finding aligns with the coupling processes between SST and SSH described by the delayed oscillator theory of ENSO. Notably, our study uncovers that incorporating this information into LSTM models extends the effectiveness of the SST + SSH coupling in ENSO forecasts up to 18 months in advance.

In Figure 6b, the lead-lagged correlations between the ONI and the SST anomalies within the western North Pacific region (averaged between 10°S–30°N across the Pacific) are illustrated. The correlations demonstrate that positive SST anomalies appear in the central Pacific (160°E–150°W) at least 18 months before the ONI peaks. The location of the leading warming signal aligns with the region where the extratropical SST anomalies, described in the seasonal footprint mechanism, enters the tropical Pacific to trigger El Niño events. Furthermore, the correlations indicate that the warm SST anomalies in the central Pacific are accompanied by cold SST anomalies in the northwestern Pacific (90°–140°E), which covers most of the area where the WNP index is defined. Previous studies have indicated that cold SST anomalies over the western North Pacific (negative WNP index) can stimulate an anomalous cyclonic circulation above, leading to anomalous westerlies over the tropical western Pacific. This anomalous circulation, in turn, induces anomalous westerlies over the tropical western Pacific, exciting downwelling Kelvin waves propagating eastward and triggering an El Niño event. Thus, SST anomalies associated with the WNP index involve both extratropical and tropical triggering processes of ENSO. This index possesses the prediction potential associated with both the tropical and extratropical ENSO dynamics. It is this unique property of the WNP index that enables the LSTM model to produce better ONI forecasts compared to all other predictors considered in this study.

The lead-lagged correlations between the ONI and SST anomalies over the north tropical Atlantic region (averaged between EQ and 15°N; Figure 6c) show that significant cold SST anomalies appear in the tropical North Atlantic (70°–50°W) approximately 18 months prior to the peak of the ONI. Previous studies have demonstrated that cold SST anomalies in the north tropical Atlantic during February–March–April can trigger central Pacific El Niño events during the subsequent winter through an extratropical teleconnection between the NTA region and the northeastern Pacific (Ham et al., 2013a, 2013b; Wang et al., 2017). This interbasin interaction is evident in Figure 6c, where warm SST anomalies emerge in the northeastern Pacific (90°–70°W) at a lag of 8 months after the appearance of cold anomalies in the Atlantic (70°–50°W), occurring as early as 18 months prior (−18 months). The warm SST anomalies in the northeastern Pacific can then propagate southwestward into the tropical central Pacific, triggering an El Niño event. The time difference between the peak season of the NTA SST anomalies (i.e., March–April–May) and the peak time of ENSO (i.e., December–January–February) is approximately 18 months. This time lag explains why the NTA index can provide prediction skill for El Niño forecasts at an 18-month lead.

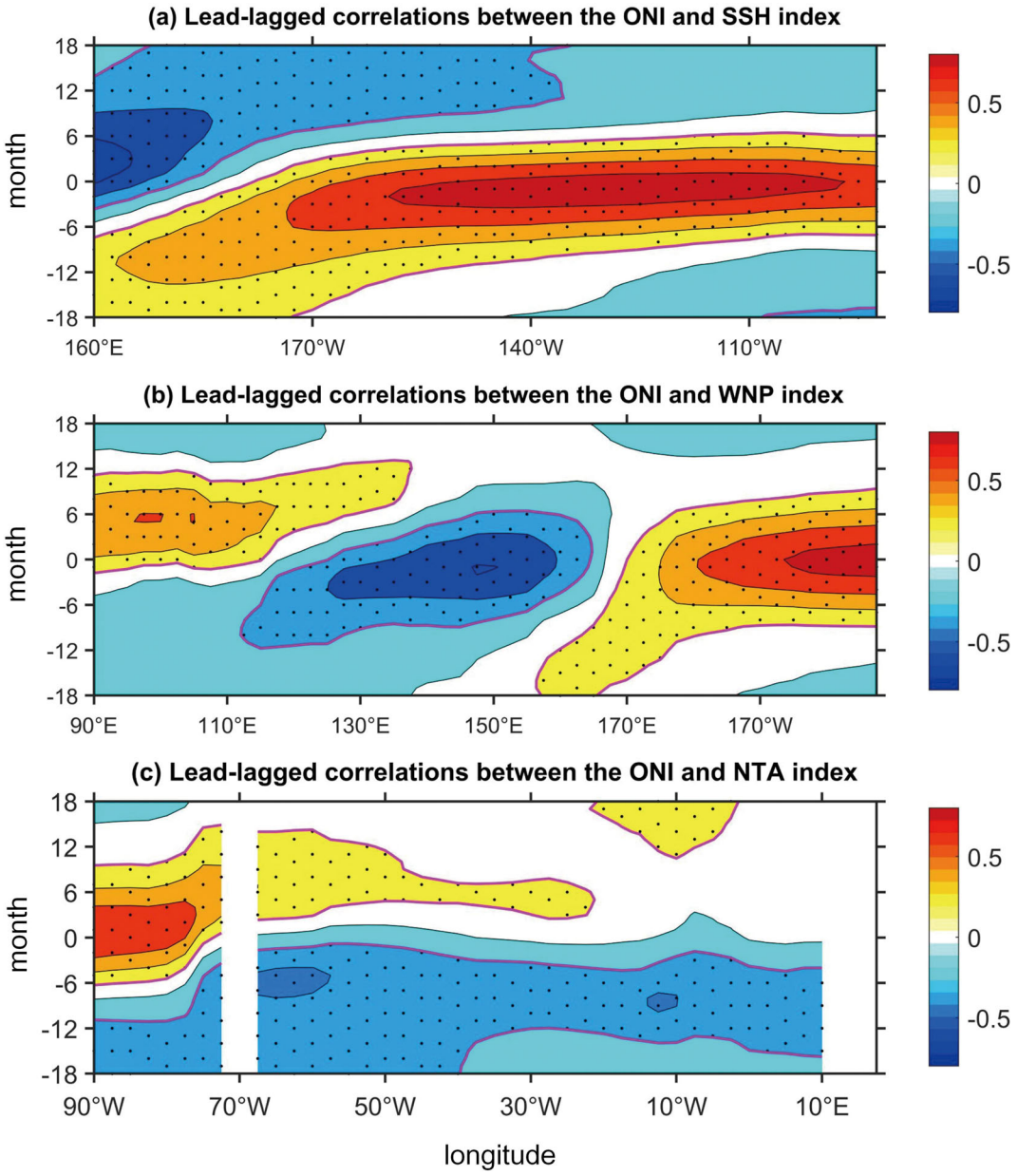

FIGURE 6 Lead-lagged correlations between the Ocean Niño Index (ONI) and the following variables: (a) sea surface height (SSH) anomalies along the equatorial (5°S–5°N) eastern-to-central Pacific, (b) sea surface temperature (SST) anomalies averaged between 10°S and 30°N across the Pacific and (c) SST anomalies averaged between 0°N and 15°N over the eastern Pacific and North Tropical Atlantic (NTA) Oceans during the period of 1982–2019. The *x*-axis represents longitude, and the *y*-axis represents the lead (+) and lag (−) times (in months) of the predictor to the ONI. Black dots indicate significance at the 99% confidence level (Student's *t* test) [Colour figure can be viewed at wileyonlinelibrary.com]

5 | CONCLUSIONS

In this paper, we examined how multiple marine and atmospheric precursors can affect the ENSO evolution and phase transition. We showed that the LSTM algorithm of machine learning can achieve reasonable accuracy in long-lead (18 months) forecasts of the ONI. The careful selection of predictors is paramount, particularly considering the multitude of extratropical mechanisms that have been proposed as potential precursors to ENSO. Extratropical predictors exhibit greater capability in extending the forecast skill of long-lead ENSO forecasting compared to tropical predictors. Among all the predictors considered, the WNP index demonstrates the highest prediction skill in ONI forecasts, followed by the NTA index and then the sea surface height index This superiority can be attributed to the involvement of SST anomalies in the WNP region in both tropical and extratropical ENSO

dynamics, allowing for the utilization of predictive potential from both components of ENSO dynamics. Overall, our findings offer insight into a group of extratropical variability patterns that may serve as effective predictors of the consecutive-year evolution of ENSO.

Our results should be interpreted with caution, as there are several limitations to consider. First, we employed multiple marine and atmospheric variables in both the linear regression model and the machine learning model. However, utilizing a dataset based on 48 years of observations may not adequately capture interannual variability. To gain a better understanding of longer timescale variability, further experiments are required. Furthermore, the evolution and progression of diverse El Niño or La Nina phenomena have been seldom explored and forecasted using multiple marine and atmospheric variables. Considering that energy transportation among different variables and Earth subsystems can potentially explain climate changes, it is crucial to investigate these aspects in future research. By delving into these areas, we can enhance our understanding of climate dynamics and improve forecasting capabilities.

AUTHOR CONTRIBUTIONS

Wan-Jiao Song: Methodology; writing – original draft; funding acquisition. **Jin-Yi Yu:** Writing – review and editing; funding acquisition; writing – original draft. **Tao Lian:** Funding acquisition; writing – review and editing.

ACKNOWLEDGEMENTS

We thank two anonymous reviewers and Editor for their valuable comments. This research is supported by the National Natural Science Foundation of China (No. 41801355) and the Open Fund of State Key Laboratory of Satellite Ocean Environment Dynamics, Second Institute of Oceanography, MNR (No. QNHX2213). Jin-Yi Yu is supported by National Science Foundation's Climate and Large-Scale Dynamics Program of the United States of America under grants AGS-2109539.

CONFLICT OF INTEREST STATEMENT

The authors declare no conflicts of interest.

DATA AVAILABILITY STATEMENT

These data were collected and made freely available by the National Oceanic and Atmospheric Administration, National Centers for Environmental Prediction-National Centre for Atmospheric Research (NCEP-NCAR) and Global Ocean Data Assimilation System. The Ocean Niño Index was provided by the National Oceanic and Atmospheric Administration National Centers for Environmental Prediction (https://origin.cpc.ncep.noaa.gov/products/analysis_monitoring/ensostuff/ONI_v5.php).

ORCID

Wan-Jiao Song https://orcid.org/0000-0003-3236-5824
Jin-Yi Yu https://orcid.org/0000-0001-6156-7623

REFERENCES

Barnston, A.G., Tippett, M.K. & Heureux, M.L. (2012) Skill of real time seasonal ENSO model predictions during 2002–11 is our capability increasing? *Bulletin of the American Meteorological Society*, 93(5), 631–651. Available from: https://doi.org/10.1175/BAMS-D-11-00111.2

Barnston, A.G., Tippett, M.K., Ranganathan, M. & LHeureux, M.L. (2019) Deterministic skill of ENSO predictions from the North American multimodel ensemble. *Climate Dynamics*, 53(12), 7215–7234. Available from: https://doi.org/10.1007/s00382-017-3603-3

Battisti, D.S. & Hirst, A.C. (1989) Interannual variability in a tropical atmosphere-ocean model: influence of the basic state, ocean geometry and nonlinearity. *Journal of the Atmospheric Sciences*, 46, 1687–1712. Available from: https://doi.org/10.1175/1520-0469(1989)046<1687:IVIATA>2.0.CO;2

Behringer, D. & Xue, Y. (2004) Evaluation of the global ocean data assimilation system at NCEP: The Pacific Ocean. In: *AMS 84th annual meeting*. Seattle, WA: AMS.

Bruce, T.A., Renellys, C.P. & Alicia, K. (2013) Triggering of El Niño onset through trade wind–induced charging of the equatorial Pacific. *Geophysical Research Letters*, 40, 1212–1216. Available from: https://doi.org/10.1002/grl.50200

Cane, M.A. & Zebiak, S.E. (1985) A theory for El Niño and Southern Oscillation. *Science*, 288, 1085–1087. Available from: https://doi.org/10.1038/s41598-020-57853-7

Capotondi, A., Wittenberg, A.T., Newman, M., Di Lorenzo, E., Yu, J.-Y., Braconnot, P. et al. (2015) Understanding ENSO diversity. *Bulletin of the American Meteorological Society*, 96(6), 921–938. Available from: https://doi.org/10.1175/BAMS-D-13-00117.1

Chen, N., Gilani, F. & Harlim, J. (2021) A Bayesian machine learning algorithm for predicting ENSO using short observational time series. *Geophysical Research Letters*, 48(17), e2021GL093704. Available from: https://doi.org/10.1029/2021GL093704

Di Lorenzo, E., Cobb, K.M., Furtado, J.C., Schneider, N., Anderson, B.T., Bracco, A. et al. (2010) Central Pacific El Niño and decadal climate change in the North Pacific Ocean. *Nature Geoscience*, 3, 762–765.

Ding, R., Li, J. & Tseng, Y. (2015) The impact of South Pacific extratropical forcing on ENSO and comparisons with the North Pacific. *Climate Dynamics*, 44(7–8), 2017–2034. Available from: https://doi.org/10.1007/s00382-014-2303-5

Guo, Y., Cao, X. & Liu, B. (2020) El Niño index prediction using deep learning with ensemble empirical mode decomposition. *Symmetry*, 12(6), 893. Available from: https://doi.org/10.3390/sym12060893

Gupta, M., Kodamana, H. & Sandeep, S. (2022) Prediction of ENSO beyond spring predictability barrier using deep convolutional LSTM networks. *IEEE Geoscience and Remote Sensing Letters*, 19, 1501205. Available from: https://doi.org/10.1109/LGRS.2020.3032353

Ham, Y., Kug, J. & Park, J. (2013a) Two distinct roles of Atlantic SSTS in ENSO variability north tropical Atlantic SST and Atlantic Niño. *Geophysical Research Letters*, 40(15), 4012–4017. Available from: https://doi.org/10.1002/grl.50729

Ham, Y., Kug, J. & Park, J. (2013b) Sea surface temperature in the north tropical Atlantic as a trigger for El Niño/Southern Oscillation events. *Nature Geoscience*, 6(2), 112–116. Available from: https://doi.org/10.1038/ngeo1686

He, Z., Gao, S., Xiao, L., Liu, D., He, H. & Barber, D. (2017) Wider and deeper cheaper and faster: Tensorized LSTMs for sequence learning. *Proc. Adv. Neural Inf. Process. Syst.*, 2017, 1–11. Available from: https://doi.org/10.48550/arXiv.1711.01577

Huang, B., Thorne, P.W., Smith, T.M., Liu, W., Lawrimore, J., Banzon, V.F. et al. (2016) Further exploring and quantifying uncertainties for extended reconstructed sea surface temperature (ERSST) version 4 (v4). *Journal of Climate*, 29, 3119–3142. Available from: https://doi.org/10.1175/JCLI-D-15-0430.1

Huang, A., Westhoff, B.V. & Sriver, R.L. (2019) Analyzing El Niño–Southern Oscillation predictability using long-short-term-memory models. *Earth and Space Science*, 6, 212–221.

Huang, P. & Xie, S. (2015) Mechanisms of change in ENSO-induced tropical Pacific rainfall variability in a warming climate. *Nature Geoscience*, 8(12), 922–926. Available from: https://doi.org/10.1029/2018EA000423

Jin, E.K. & Kinter, J.L. (2009) Characteristics of tropical Pacific SST predictability in coupled GCM forecasts using the NCEP CFS. *Climate Dynamics*, 32(5), 675–691. Available from: https://doi.org/10.1007/s00382-008-0418-2

Jin, F.F. (1997) An equatorial recharge paradigm for ENSO, I. Conceptual model. *Journal of the Atmospheric Sciences*, 54, 811–829. Available from: https://doi.org/10.1175/1520-0469(1997)0542.0.CO;2

Kalnay, E., Kanamitsu, M. & Kistler, R. (1996) The NCEP/NCAR 40-year reanalysis project. *Bulletin of the American Meteorological Society*, 77(3), 437–471. Available from: https://doi.org/10.1175/1520-0477(1996)077<0437:TNYRP>2.0.CO;2

Kao, H.Y. & Yu, J.Y. (2009) Contrasting eastern-Pacific and central-Pacific types of ENSO. *Journal of Climate*, 22, 615–632.

Latif, M., Anderson, D., Barnett, T., Cane, M., Kleeman, R., Leetmaa, A. et al. (1998) A review of the predictability and prediction of ENSO. *Journal of Geophysical Research: Oceans*, 103(C7), 14375–14393. Available from: https://doi.org/10.1029/97JC03413

Liebmann, B. & Smith, C.A. (1996) Description of a complete (interpolated) outgoing longwave radiation dataset. *Bulletin of the American Meteorological Society*, 77(6), 1275–1277. Available from: https://doi.org/10.1175/1520-0477(1996)077<1255:EA>2.0.CO;2

Ma, L.H., Han, Y.B. & Yin, Z.Q. (2010) Quasi-biennial oscillation signals in outgoing long-wave radiation of the equator. *Advances in Space Research*, 46(11), 1477–1481. Available from: https://doi.org/10.1016/j.asr.2010.07.020

McPhaden, M.J., Timmermann, A., Widlansky, M.J., Balmaseda, M.A. & Stockdale, T.N. (2015) The curious case of the El Niño that never happened: a perspective from 40 years of progress in climate research and forecasting. *Bulletin of the American Meteorological Society*, 96(10), 1647–1665.

Neelin, J.D. (1991) The slow sea surface temperature mode and the fast-wave limit: Analysis theory for tropical interannual oscillations and experiments in a hybrid coupled model. *Journal of Atmospheric Sciences*, 48, 584–606. Available from: https://doi.org/10.1175/1520-0469(1991)048<0584:TSSSTM>2.0.CO;2

Nooteboom, P.D., Feng, Q.Y. & López, C. (2018) Using network theory and machine learning to predict El Niño. *Earth System Dynamics*, 9(3), 969–983. Available from: https://doi.org/10.5194/esd-9-969-2018

Pegion, K., Selman, C.M. & Larson, S. (2020) The impact of the extratropics on ENSO diversity and predictability. *Climate Dynamics*, 54(9–10), 4469–4484. Available from: https://doi.org/10.1007/s00382-020-05232-3

Philander, S.G.H. (1998) *Is the temperature rising? The uncertain science of global warming*. Princeton, NJ: Princeton University Press, p. 250.

Qin, J., Ding, R. & Wu, Z. (2017) Relationships between the extratropical ENSO precursor and leading modes of atmospheric variability in the Southern Hemisphere. *Advances in Atmospheric Sciences*, 34(3), 360–370. Available from: https://doi.org/10.1007/s00376-016-6016-z

Ren, H., Zuo, J. & Deng, Y. (2019) Statistical predictability of Niño indices for two types of ENSO. *Climate Dynamics*, 52, 5361–5382. Available from: https://doi.org/10.1007/s00382-018-4453-3

Srivastava, N., Hinton, G. & Krizhevsky, A. (2014) Dropout a simple way to prevent neural networks from overfitting. *Journal of Machine Learning Research*, 15, 1929–1958.

Suarez, M.J. & Schopf, P.S. (1988) A delayed action oscillator for ENSO. *Journal of the Atmospheric Sciences*, 45, 3283–3287. Available from: https://doi.org/10.1175/1520-0469(1988)0452.0.CO;2

Timmermann, A., An, S. & Kug, J. (2018) El Niño–Southern Oscillation complexity. *Nature*, 559(7715), 535–545. Available from: https://doi.org/10.1038/s41586-018-0252-6

Trenberth, K.E. & Stepaniak, D.P. (2001) Indices of El Niño evolution. *Journal of Climate*, 14(8), 1697–1701. Available from: https://doi.org/10.1175/1520-0442(2001)014<1697:LIOENO>2.0.CO;2

Vimont, J.D., Wallace, M.J. & Battisti, S.D. (2003) The Seasonal Foot printing Mechanism in the Pacific: Implications for ENSO. *Journal of Climate*, 16(16), 2668–2675. Available from: https://doi.org/10.1175/1520-0442(2003)016<2668:TSFMIT>2.0.CO;2

Wang, C.Z. (2018) A review of ENSO theories. *National Science Review*, 5, 813–823. Available from: https://doi.org/10.10938/nsr/nwy104

Wang, L., Yu, J.-Y. & Paek, H. (2017) Enhanced biennial variability in the Pacific due to Atlantic capacitor effect. *Nature Communications*, 8, 14887. Available from: https://doi.org/10.1038/ncomms14887

Wang, S., Heureux, M. & Chia, H. (2012) ENSO prediction one year in advance using western North Pacific sea surface temperatures. *Geophysical Research Letters*, 39(5), L5702. Available from: https://doi.org/10.1029/2012GL050909

Yu, J.-Y. & Fang, S.-W. (2018) The distinct contributions of the seasonal footprinting and charged-discharged mechanisms to ENSO complexity. *Geophysical Research Letters*, 45, 6611–6618. Available from: https://doi.org/10.1029/2018GL077664

Yu, J.-Y. & Kao, H.-Y. (2007) Decadal changes of ENSO persistence barrier in SST and ocean heat content indices: 1958–2001. *Journal of Geophysical Research*, 112, D13106. Available from: https://doi.org/10.1029/2006JD007654

Yu, J.-Y., Kao, H.-Y. & Lee, T. (2010) Subtropics-related interannual sea surface temperature variability in the equatorial central

Pacific. *Journal of Climate*, 23, 2869–2884. Available from: https://doi.org/10.1175/2010JCLI3171.1

Yu, J.-Y. & Kim, S.T. (2011) Relationships between extratropical sea level pressure variations and the central-Pacific and eastern-Pacific types of ENSO. *Journal of Climate*, 24, 708–720. Available from: https://doi.org/10.1175/2010JCLI3688.1

Yu, J.-Y., Lu, M.-M. & Kim, S.T. (2012) A change in the relationship between tropical central Pacific SST variability and the extratropical atmosphere around 1990. *Environmental Research Letters*, 7, 034025. Available from: https://doi.org/10.1088/1748-9326/7/3/034025

Yu, J.-Y., Wang, X., Yang, S., Paek, H. & Chen, M. (2017) The changing El Niño–Southern Oscillation and associated climate extremes. In: Wang, S.-Y., Yoon, J.-H., Funk, C. & Gillies, R.R. (Eds.) *Climate extremes: patterns and mechanisms*. *AGU Geophysical Monograph Series*. Washington, D.C: American Geophysical Union and John Wiley & Sons, Inc; Vol. 226. AGU, pp. 3–38.

Zhang, H., Clement, A. & Di Nezio, P. (2014) The South Pacific meridional mode: a mechanism for ENSO-like variability. *Journal of Climate*, 27, 769–783. Available from: https://doi.org/10.1175/JCLI-D-13-00082.1

Zhao, Y., Di Lorenzo, E., Sun, D. & Stevenson, S. (2021) Tropical Pacific decadal variability and ENSO precursor in CMIP5 models. *Journal of Climate*, 34, 1023–1045. Available from: https://doi.org/10.1175/JCLI-D-20-0158.1

How to cite this article: Song, W.-J., Yu, J.-Y., & Lian, T. (2023). The efficacy of tropical and extratropical predictors for long-lead El Niño-Southern Oscillation prediction: A study using a machine learning algorithm. *International Journal of Climatology*, 1–13. https://doi.org/10.1002/joc.8241